remote sensing

Article

Quantifying the Actual Impacts of Forest Cover Change on Surface Temperature in Guangdong, China

Wenjuan Shen [1,2,*], Jiaying He [3], Chengquan Huang [3] and Mingshi Li [1,2]

1 College of Forestry, Nanjing Forestry University, Nanjing 210037, China; nfulms@njfu.edu.cn
2 Co-Innovation Center for Sustainable Forestry in Southern China, Nanjing Forestry University, Nanjing 210037, China
3 Department of Geographical Sciences, University of Maryland, College Park, MD 20742, USA; hjy0608@terpmail.umd.edu (J.H.); cqhuang@umd.edu (C.H.)
* Correspondence: wjshen@njfu.edu.cn; Tel.: +86-25-8542-7327

Received: 14 June 2020; Accepted: 21 July 2020; Published: 22 July 2020

Abstract: Forest cover change is critical in the regulation of global and regional climate change through the alteration of biophysical features across the Earth's surface. The accurate assessment of forest cover change can improve our understanding of its roles in the regulation processes of surface temperature. In spite of this, few researchers have attempted to discern the varying effects of multiple satellite-derived forest changes on local surface temperatures. In this study, we quantified the actual contributions of forest loss and gain associated with evapotranspiration (ET) and albedo to local surface temperature in Guangdong Province, China using an improved spatiotemporal change pattern analysis method, and explored the interrelationships between surface temperature and air temperature change. We specifically developed three forest change products for Guangdong, combining satellite observations from Landsat, PALSAR, and MODIS for comparison. Our results revealed that the adjusted simple change detection (SCD)-based Landsat/PALSAR forest cover data performed relatively well. We found that forest loss and gain between 2000 and 2010 had opposite effects on land surface temperature (LST), ET, and albedo. Forest gain led to a cooling of −0.12 ± 0.01 °C, while forest loss led to a warming of 0.07 ± 0.01 °C, which were opposite to the anomalous change of air temperature. A reduced warming to a considerable cooling was estimated due to the forest gain and loss across latitudes. Specifically, mid-subtropical forest gains increased LST by 0.25 ± 0.01 °C, while tropical forest loss decreased LST by −0.16 ± 0.05 °C, which can demonstrate the local differences in an overall cooling. ET induced cooling and warming effects were appropriate for most forest gain and loss. Meanwhile, the nearby temperature changes caused by no-change land cover types more or less canceled out some of the warming and cooling. Albedo exhibited negligible and complex impacts. The other two products (i.e., the GlobeLand30 and MCD12Q1) affect the magnitude of temperature response due to the discrepancies in forest definition, methodology, and data resolution. This study highlights the non-negligible contributions of high-resolution maps and a robust temperature response model in the quantification of the extent to which forest gain reverses the climate effects of forest loss under global warming.

Keywords: forest change; change detection estimates; surface temperature; actual impacts; biophysical features

1. Introduction

Forest cover change can exert substantial impacts on climate conditions by affecting carbon budget and energy balance [1–5]. Numerous observational and modeling studies have been conducted to understand these impacts [6–8]. Surface temperature is a key variable for measuring the environmental change of the underlying surface. It plays an important role in the heat and energy exchange between the surface and the atmosphere [9]. Moreover, the same forest change activities are driven by varying biophysical mechanisms associated with changes in ET, albedo, and surface roughness in different regional climate conditions from north to south, which regulate the temperature change [3,10].

Traditional statistical methods based on land-use change and site observations have been commonly utilized to explore temperature fluctuations [11,12]. Weather stations and field sites tend to be sparsely distributed, however, and therefore cannot accurately depict the spatiotemporal change pattern of the temperature change related to forest cover dynamics. Clearly, quantifying the spatial effects of forest cover change on surface temperature at both fine and large scales would improve our understanding of the biophysical interaction mechanisms between forest and climate and support forest ecosystem management during climate change [10,13,14].

A variety of satellite-based datasets describing forest cover and climate variables as well as their changes have been developed and applied in site-based pairs and individual time-based statistical modeling methods [15,16]. Forest change can significantly affect surface temperature, and the area, magnitude, and direction of any changes vary significantly from local to global scales [7,17,18]. Some studies have found the inconsistent warming or cooling effects of forest change on temperature [7,19–21]. For example, forest cooling becomes more obvious as latitude decreases, but planted forests replacing natural forests will reduce ET and thus reduce biophysical cooling [22]. These inconsistent changes are more heterogeneous at regional scale and have caused debates among researchers and management communities of forest or climate [23].

Multi-temporal satellite observations have been commonly utilized to evaluate the biophysical impacts of forest change on surface temperature [15,17,24]. In particular, the space-for-time method has received the most attention and application [5,25]. This method considers pairing the sample-based forests and other land cover types as well as space-based and time-based temperatures with similar climate forcing. The land use changes originate from the potential forest activities, as well as having an environmental background that is based on long-term averages of observations that would overestimate the surface temperature [5]. This approach has been refined in order to quantify the potential effects of the hypothetical land use change (i.e., no change between land cover types) and the effects of the actual change (i.e., land cover change minus local no-change in two time periods) on surface temperature [15]. Sampling scales for the change estimation, such as moving window size, circle area, or even larger sizes, have been utilized [18,24,26]. In actuality, the conversion from forest to other types between different years would have different impacts on both the sign and magnitude of the surface temperature [17,27]. Further changes to the background properties could also affect the temperature variations of forests; for example, a cooling effect can be detected in warmer regions (e.g., the tropics) and a warming effect can be found in cooler regions (e.g., high latitudes or elevations) [23,28]. Thus, it is necessary to take the actual changes of both forest cover and local surrounding land types into account when assessing the local impacts of forest cover change.

Many studies have utilized the space-for-time method to investigate local impacts based on hypothetical forest change using forest and adjacent open land types developed with coarse-resolution satellite data such as MODIS [16,23–25]. These types of global land cover maps are typically characterized by low accuracy, particularly in regions with heterogeneous land cover [29]. Forest or land cover changes extracted from high-resolution satellite data, such as the historical Landsat archive, have also been adopted for assessing the impacts of these changes on surface temperature [18,30]. Even though applications of long-term Landsat data on a large scale can be difficult due to data matching issues with observations from other sources (e.g., modeling and in-situ observations) [18], high-resolution maps developed with Landsat are still recommended to assess the impacts of forest change on temperature [27,31]. The accuracy of remote sensing-based forest dynamic changes is definitely a function of data source, definition, and algorithms [32,33]. For example, direct usage of the threshold-based global dataset or simply subtracting the percentage forest cover values over two years would lead to the biased evaluation of forest change associated with temperature [15,18].

Few studies, however, have attempted to compare and quantify how different forest change results affect regional climate.

These data or datasets were developed for a variety of purposes in forest and climate studies [18,26]. For example, China's global land cover data (GlobeLand30) aim to achieve high overall accuracy for classifying multiple land cover types [34], while Japan's PALSAR mosaic data focus on distinguishing forest and non-forest classes [35]. They are rarely utilized in assessing fine-scale temperature variations in local regions, however, such as important climate areas along the Maritime Silk Road. Consequently, a fully integrated solution that incorporates multi-source satellite remote sensing-based forest change products, which originated from various data sources and employed different methodologies, accuracies, and scales, is needed to explain the temperature responses to actual forest change.

In this study, we focused on quantifying the actual impacts of forest change on local surface temperature across Guangdong Province, China, using three sets of product-based forest cover changes from 2000–2010. Specifically, we attempted to: (1) Detect forest loss and gain based on two change detection methods—adjusted simple change detection (adjusted SCD) and morphological change detection (MCD)—with three forest cover products developed from Landsat, PALSAR, and MODIS (30-m–1-km) data; (2) improve the actual forest change estimations and their impacts on surface temperature using the improved spatiotemporal pattern change trend method by eliminating the effect of surrounding no-change mechanisms; and (3) quantify the impacts of multiple forest change caused by multi-source datasets associated with ET and albedo on local surface temperature, as well as their interrelationships between surface temperature and air temperature

2. Data and Methods

2.1. Study Area

The study area (20°13′N–25°31′N, 109°39′E–117°19′E) is Guangdong Province in southern China, mainly spanning three forest zones within the latitudinal climate, namely mid-subtropical typical evergreen broadleaved forests, south-subtropical monsoon evergreen broadleaved forests, and tropical monsoon forest or rainforest. The annual mean precipitation is 1300–2500 mm, and the temperature ranges from 19–24 °C. There are a large number of planted forests and irrigated farmland in northern and southern Guangdong, respectively. Moreover, as an important link of the Maritime Silk Road, Guangdong Province is conducive to strengthening cooperation with countries along the route in addressing climate change on a regional scale.

2.2. Forest Cover Datasets

We obtained the forest cover data (Figure 1) for 2000 and 2010 from three sources: China's 30-m global land cover data (GlobeLand30) [34], the 30-m forest/non-forest (FNF) product developed with Landsat and PALSAR data [36], and the 500-m MODIS International Geosphere-Biosphere Programme (IGBP) land cover dataset [37]. The GlobeLand30 was developed by integrating pixel-based and object-based methods using a pixel-object-knowledge-based (POK-based) operational approach. The FNF product was generated by combining the Landsat-based cumulative maximum normalized difference vegetation index (NDVI) with PALSAR-based stochastic gradient boosting (SGB) classification. The MODIS land cover product (MCD12Q1: MODIS LC) was implemented using a hierarchical classification model and a hidden Markov model.

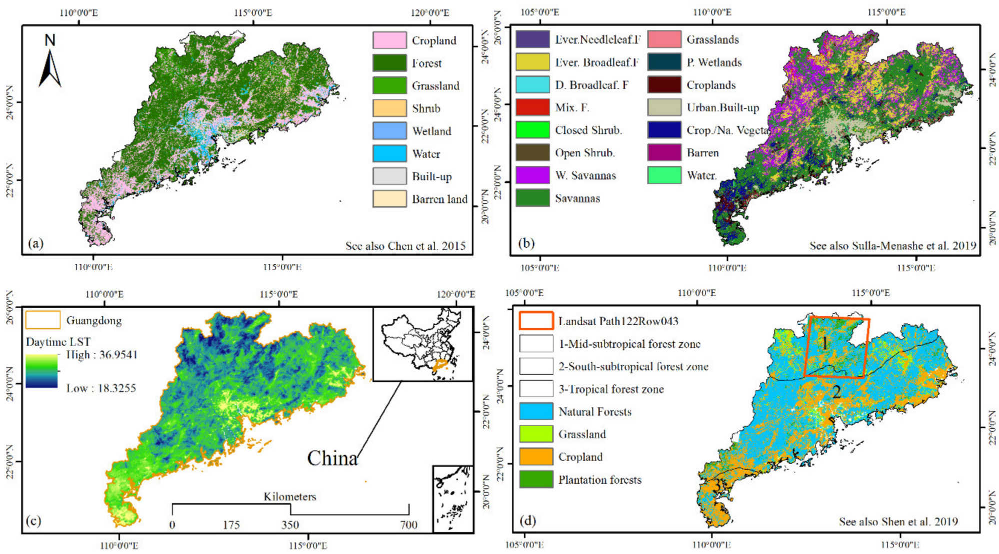

Figure 1. Forest cover data from (**a**) GlobeLand30, (**b**) MCD12Q1, and (**d**) Landsat/PALSAR-based forest/non-forest (FNF) in 2010, as well as (**c**) the average MODIS daytime LST from 2007–2010 in Guangdong, China.

For each product, we combined all forest types into the "forest" domain and all other types into the "non-forest" domain (Figure 2a). We upscaled the original values at 30-m and 500-m resolutions to 1-km resolution using the bilinear interpolation resampling method in order to match the resolution of the MODIS LST, ET, and albedo data (Table 1).

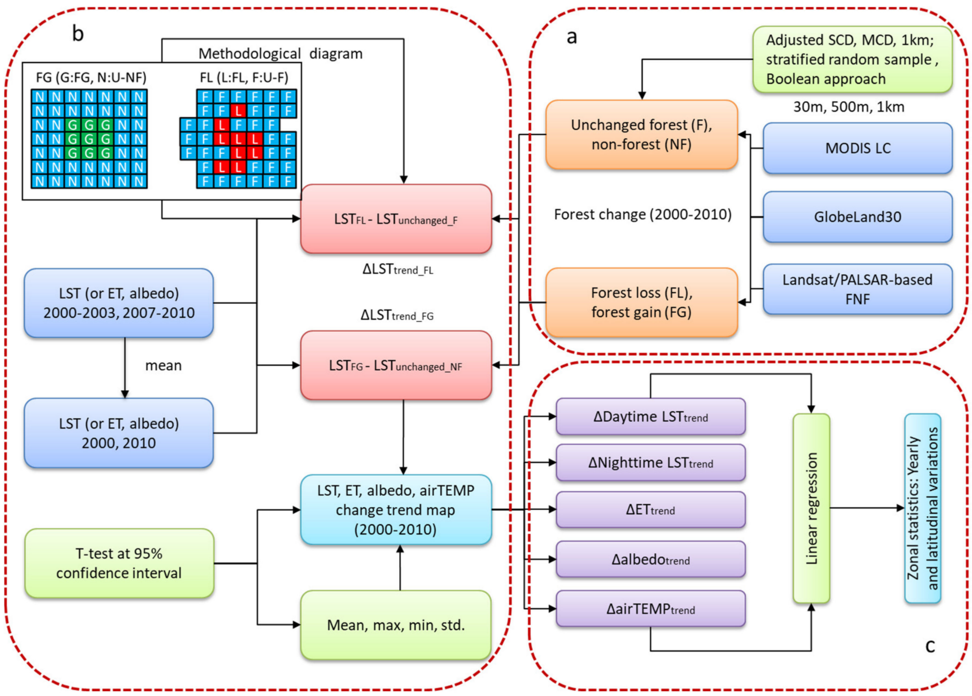

Figure 2. Workflow diagram of actual change used to analyze the yearly change differences in daytime and nighttime land surface temperature (LST), evapotranspiration (ET), and albedo of forest loss (FL: "L") and forest gain (FG: "G") from 2000–2010 based on the improved spatial pattern change method (N: U-NF, "no-change non-forest"; F: U-F, "no-change forest"). (**a**): Three dataset-based forest change data; (**b**): An improved spatiotemporal analysis method for LST change due to forest cover change; (**c**): The relationship between the yearly change differences in daytime and nighttime LST, ET, and albedo of forest change and their spatio-temporal statistical analysis.

Table 1. Summary of different satellite-based land cover products used for forest cover change estimates.

Dataset	Source	Forest Definition	Overall Accuracy	Reference
GlobeLand30	Landsat-like	Canopy cover > 30% (including sparse woods over 10–30%)	84%–89%	[34]
SGB-NDVI/FNF	Landsat/PALSAR	Canopy cover > 10%	83%–86%	[36]
MCD12Q1	MODIS	Tree height > 2 m, tree cover > 60%	74%	[37]

2.3. *Estimation of Forest Cover Change*

2.3.1. Forest Loss and Gain Characterization

We used three satellite-based datasets to monitor forest loss and gain in Guangdong. Two post-classification change detection algorithms (MCD and adjusted SCD) were compared to estimate the increase or decrease in forest cover (Figure 2a).

The MCD algorithm [38] consists of 3 major steps. First, a simple overlay of the forest maps is created. Second, areas in which changes occur with high probability are identified, setting a two-pixel edge width threshold (i.e., 30-m or 1-km resolution pixels) and removing all change objects less than or equal to twice the edge width (4×4 pixels). Third, change objects are reconstructed by dilation with a kernel of 3×3 pixels to exclude unreliable changes, and a morphological opening procedure is used to remove branches from the resulting dilated change objects. Ultimately, homogeneous and contiguous gain and loss objects are obtained by the MCD algorithm.

For the implementation of the adjusted SCD algorithm, we defined forest loss as a forest pixel in the first period being converted to a non-forest pixel in the later period. A change in the opposite direction was defined as forest gain. After a simple overlay of two forest maps, a majority filter was applied by calculating focal values for the neighborhood of the default moving window (3×3 pixels) in order to reduce the so-called "salt and pepper" issue. A mathematical morphology opening operation (3×3 pixels) was then selected to eliminate the speckled and smooth boundaries, and to exclude the burrs and isolated pixels.

Both algorithms are traditional post-classification change detection methods integrated with filter and morphological procedures. The largest discrepancy between the two is that MCD accounts for small errors caused by misregistration or misclassification but avoids area exclusion and maintains a high level of detail for change objects combined with morphological procedures, whereas no threshold settings are considered by the adjusted SCD. Finally, forest loss, forest gain, no-change forest, and no-change non-forest were derived. The MCD algorithm also provides spurious change types.

2.3.2. Accuracy Assessment and Area Estimation of Post-Classification Change Analysis

Historical measurements of forest loss and gain in forest inventory data seldom examined the spatiotemporal patterns of these changes explicitly. Ground visits for the reference data at the initial date in real time were not possible. Archived satellite imagery or aerial photography is available for the initial date of the change period [32], however. In order to assess the performances of the post-classification change maps produced by the MCD and adjusted SCD algorithms, we instead used the Landsat-based forest change results [36] generated by the vegetation change tracker (VCT) algorithm in northern Guangdong (Landsat Path122 Row043 footprint) (Table 2), as a reference for evaluating the estimation of forest area and accuracy. Because the VCT-based change and no-change types with an overall accuracy of 92% indicated the superior performance [39]. Specifically, the forest disturbance, forestation, persisting forest, and persisting non-forest outputs were considered as forest loss, forest gain, no-change forest, and non-forest in-situ datasets, respectively.

Table 2. Summary of field inventories and forest change products used for accuracy assessment.

Dataset	Source	Forest Definition	Overall Accuracy	Reference
NFIs	Ground, and remote sensing plot observations	Canopy cover 20%, diameter at breast height (DBH) > 5 cm		[40]
VCT	Landsat (Path122Row043)	Pixels with low IFZ values (~0) are close to the spectral center of forest samples	92%	[41,42]

We calculated the areas of forest loss and gain using the pixel statistics for all of the datasets. We then utilized a stratified random sample strategy [33] to select validation regions of interest (ROIs) for assessing the accuracy of the MCD and adjusted SCD-based forest cover change maps at both original and resampled resolutions. We identified a total of 350 random point samples for all classes, including 100 for forest loss, 100 for forest gain, 50 for no-change forest, 50 for no-change non-forest, and 50 for spurious change. These samples from the MCD (a total of 350) and adjusted SCD (a total of 300, excluding the spurious change class) for accuracy validation were selected based on very high resolution imagery available from Google Earth, national forest inventories (NFIs), and sub-compartment data for the period 2000–2010. Considering the difficulty of interpretation and potential errors, forest loss and gain patches smaller than 3×3 pixels were not used for validation [43]. We then used the equations developed by Olofsson et al. [33] to estimate the error matrix based on the sample counts and the areas computed from the class patches and proportions.

Next, we compared the spatial distribution of our forest change results using a pixel-based Boolean approach. We created agreement and disagreement maps between each of our results and the VCT-based reference data. We used the same forest loss, forest gain, no-change forest, and no-change non-forest labels for each pair of comparisons. We then quantified the areas and overall accuracy values of the agreement and disagreement maps.

2.4. Extraction of Land Surface Variables and Climate Variables

We obtained land surface temperature (LST) data from the 8-day (8 d) MODIS MYD11A2 product (2002–2010) [44]. Both Aqua-based daytime and nighttime temperatures were considered, which were closer to the lowest and highest temperatures during the day. The 8-day MODIS MOD16A2 ET (2000–2010) [45] and MCD43B3 albedo (2000–2010) [46] products corresponding to the acquisition time of the MODIS LST data were collected after data error control [26]. The means of the black sky and white sky albedo values were used. We then averaged all land surface data from 2000–2003 to represent the land surface data in 2000, and the data from 2007–2010 to represent the land surface data in 2010 (Figure 2b).

Otherwise, random forest model-based spatially interpolated air temperature maps, including annual average maximum and minimum temperatures in 2000 and 2010, were selected [26]. The point data of air temperature are from the China Meteorological Administration annual ground dataset. We found a strong correlation between the interpolated air temperature and the meteorological station-based data; the values corresponding to average maximum and minimum temperatures are 0.83/0.75 and 0.99/0.98 for 2000 and 2010, respectively. Elevation adjustment was also conducted using the linear regression equation by Li et al. [25], in order to offset the temperature biases due to elevation differences.

2.5. Spatiotemporal Analysis Method for LST Change due to Forest Cover Change

A spatiotemporal pattern change analysis method has been developed by Shen et al. [26] to quantify the actual LST change trend of afforested land. However, the temperature difference of surrounding features may be a major factor that can influence the effects of forests on temperature by altering biophysical processes, leading to differences in albedo and ET [28]. Thus, we improved this algorithm by considering the impacts of local temperature change caused by nearby land cover types on the forest change. Here, the actual forest cover change was identified as a transition from forest to non-forest or non-forest to forest, with all of the changes occurring at the pixel level within a given time period. The effects of spatial changes in forest loss and gain on the surface temperature can be quantified by calculating the difference in LST trends of forest loss (LST_{FL}) or forest gain (LST_{FG}) pixels minus the difference in LST trends of nearby unchanged forest ($LST_{unchanged\_F}$) or unchanged non-forest ($LST_{unchanged\_NF}$) (Figure 2b). The difference of forest loss and gain for MODIS daytime and nighttime LST, ET, and albedo from 2000 and 2010 can be calculated using Equations (1) and (2):

$$\Delta LST_{trend\_FL} = LST_{FL} - LST_{unchanged\_F} \tag{1}$$

$$\Delta LST_{trend\_FG} = LST_{FG} - LST_{unchanged\_NF} \tag{2}$$

Positive ΔLST_{trend_FL} and ΔLST_{trend_FG} values represent a warming effect of FL and FG, while negative values imply a cooling effect and 0 values imply no significant difference. For forest gain, forests have a cooling effect when the $LST_{unchanged\_NF}$ is higher than the LST_{FG}. Conversely, forests have a warming effect if the $LST_{unchanged\_NF}$ is lower than the LST_{FG}. Equations (1) and (2) assume that two pixels in nearby region share similar large-scale climate forcings, nonlocal signals related to natural variability will be removed, and the mean LST difference is largely attributable to forest cover change [15]. To calculate the trend difference of forest gain and loss on the surface temperature, we defined four local regions, including all of Guangdong, as well as the mid-subtropical, south-subtropical, and tropical zones. We selected sample sizes that were quite large when pairing change with nearby no-change pixels, because the varying distance limits within the reasonable range between change and no-change types was shown to have a very small impact [25]. The relationship between ΔLST_{trend_FL} (ΔLST_{trend_FG}) and ΔET_{trend_FL} (ΔET_{trend_FG}) or $\Delta albedo_{trend\_FL}$ ($\Delta albedo_{trend\_FG}$) were evaluated using the yearly difference values of changed temperature, ET, and albedo data of forest loss and gain revealed by linear regression analysis (Figure 2c). Furthermore, air temperature is closely to surface temperature, but the two have different physical meanings and influencing factors [47]. In order to better understand this issue, we then estimated the relationship between in-situ measurement-based air temperature change and two land surface temperatures of forest change using a similar model and statistical metrics (adjusted R-squared, slope, and intercept).

3. Results

3.1. Forest Area Estimates from Satellite Datasets with Different Spatial Resolution

Forest areas derived from the three satellite datasets exhibited large discrepancies (Table 3). The total forest areas from the Landsat/PALSAR-based FNF in 2000 and 2010 were relatively close to the results of the National Forestry Statistics Yearbook of China but were lower than the areas from the GlobeLand30 and higher than the areas from the MODIS LC. Forest areas showed generally high consistency between the original forest maps and the resampled forest maps, with the exception of those estimated by GlobeLand30. The Landsat/PALSAR-based FNF maps developed by Shen et al. [36] missed a small amount of forest areas near the province boundary. Overall, the forest areas of the original (30-m) and resampled (1-km) Landsat/PALSAR-based FNF maps were correspondingly consistent and reliable.

Table 3. Comparison of the forest area (unit: 10^6 ha) of three datasets with different resolutions in 2000 and 2010 in Guangdong Province.

Year	NFI	GlobeLand30 (30-m/1-km)	MCD12Q1 (500-m/1-km)	Landsat/PALSAR (30-m/1-km)
2000	8.27	9.75/4.32	3.02/3.17	6.05/5.91
2010	8.74	9.74/4.33	3.04/3.18	7.55/7.61

3.2. Forest Cover Change Estimates from Datasets with Different Spatial Resolutions

3.2.1. Assessment of Post-Classification Change Maps in Northern Guangdong

By comparing the areas of the three post-classification datasets and VCT-based forest loss and gain in northern Guangdong, we observed large discrepancies across datasets (Figure 3, Table S1). The total forest loss and gain areas from the Landsat/PALSAR-based FNF were the largest among all of the datasets, as well as the VCT-based estimation. The areas estimated by the SCD-based forest cover maps were substantially larger than the MCD-based areas. Although VCT-based results typically show high accuracy, errors could still exist for estimating forest cover change due to the different post-classification methods and resampled data.

The accuracies of the forest cover change maps in northern Guangdong yielded by the MCD and adjusted SCD algorithms at different spatial resolutions are listed in Table S2. Using the MCD algorithm, the overall accuracy levels were approximately 20–60% for the original-resolution datasets and 20–40% for the resampled datasets. The accuracies of the adjusted SCD algorithm-based results were approximately 30–70% and 30–50%, 10% higher than those generated from the lowest and highest values in the MCD algorithm. Moreover, for the producer accuracies of forest loss (FL) and gain (FG), the results from the Landsat/PALSAR-based FNF at 30-m (MCD: 50% and 57%; SCD: 57% and 49%, respectively) and 1-km spatial resolutions (MCD: 12% and 12%; SCD: 16% and 19%, respectively) were superior to those of the other two datasets, while the accuracies of forest loss and gain from the GlobeLand30 were the lowest.

Based on a pair-wise comparison of the spatial agreement between the VCT outputs and the three datasets generated in previous step, we found that the VCT-GlobeLand30 pair displayed the largest area agreements and highest overall agreement accuracies at the original resolution, developed by either the MCD or adjusted SCD (Table S3). In particular, the accuracy of VCT-GlobeLand30 reached about 80% using the adjusted SCD algorithm. The overall agreement accuracies of the resampled VCT-MCD12Q1 pair ranked the second highest, following the VCT-GlobeLand30 pair. The VCT-Landsat/PALSAR pair at the resampled 1-km resolution developed by the adjusted SCD performed best, exhibiting a 67% agreement accuracy. The overall Boolean agreement of forest cover change revealed better coincidence between VCT and Landsat/PALSAR than other pairs after resampling, while the overall accuracies used for the spatial agreement of forest loss and gain were lower than those of no-change forest (PF) and non-forest (PNF) types (Table S3).

In summary, the Landsat/PALSAR-based forest cover change maps were superior to the other datasets-based maps in terms of the overall accuracy, Kappa coefficient, and spatial agreement, especially when using the adjusted SCD algorithm (Tables S2 and S3). Although resampling the 30-m Landsat/PALSAR-based results (66%) to 1-km (41%) reduced the accuracy (Table S2), the overall performance was still higher than the results from the other two datasets.

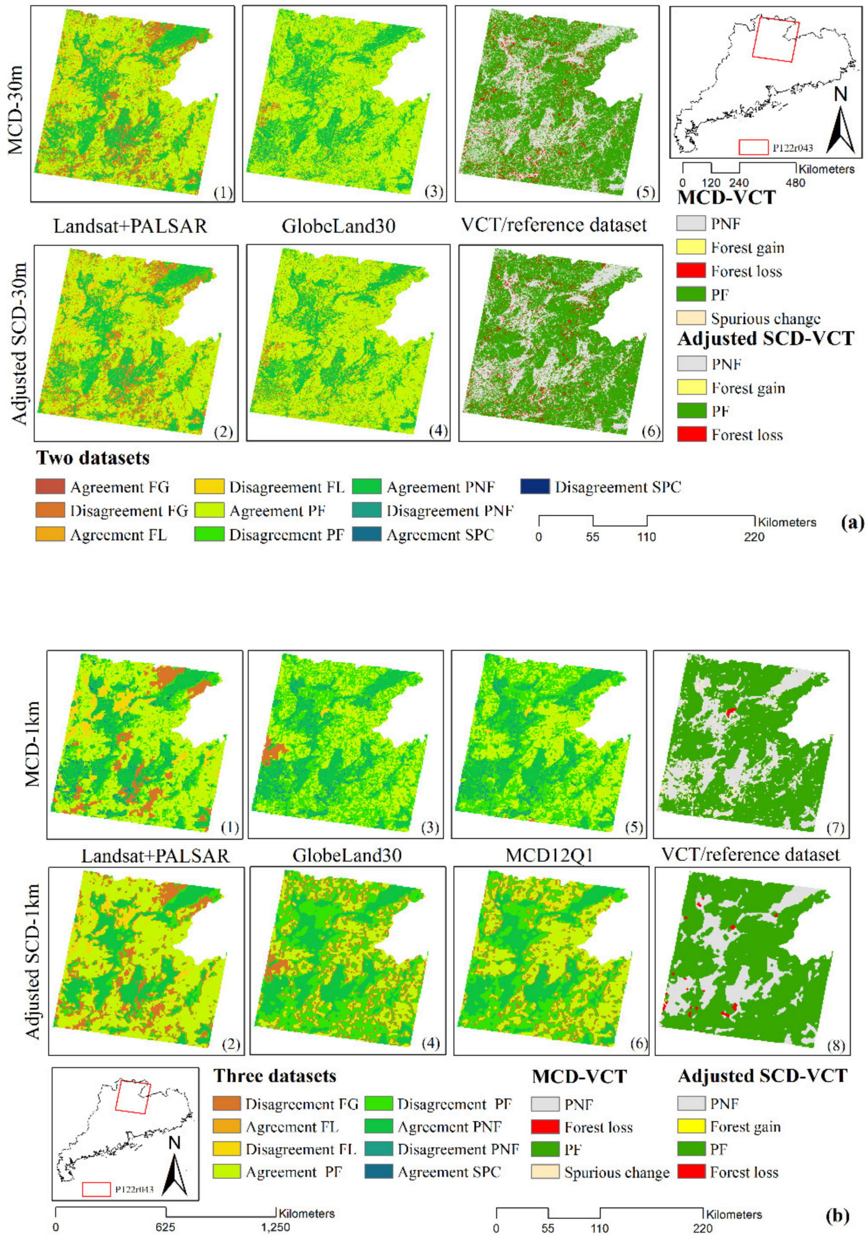

Figure 3. Maps of forest cover change (p122r043) spatial agreement (SA) and disagreement (SD) assessments at 30-m resolution ((**a**)-1, 2, 3, 4) and 1-km resolution ((**b**)-1, 2, 3, 4, 5, 6) using the VCT-based results ((**a**)-5, 6 and ((**b**)-7,8) as a reference dataset among the algorithm-based datasets.

3.2.2. Analysis of Forest Cover Change in Guangdong Province

The forest cover change based on three satellite datasets from 2000–2010 was mapped and summarized using the MCD and SCD methods (Figures 4 and 5, Figure S1). The resampled map from the Landsat/PALSAR-based FNF generated the largest forest change area. It exhibited that higher spatial consistency than the other datasets at the same resolution, which was in agreement with the VCT-based validation results in Section 3.2.1. For the maps developed with the two change detection methods, we observed a small spatially estimated discrepancy for each individual dataset at the same resolution. Generally, the total forest cover area estimated by the adjusted SCD was larger than the area estimated by the MCD.

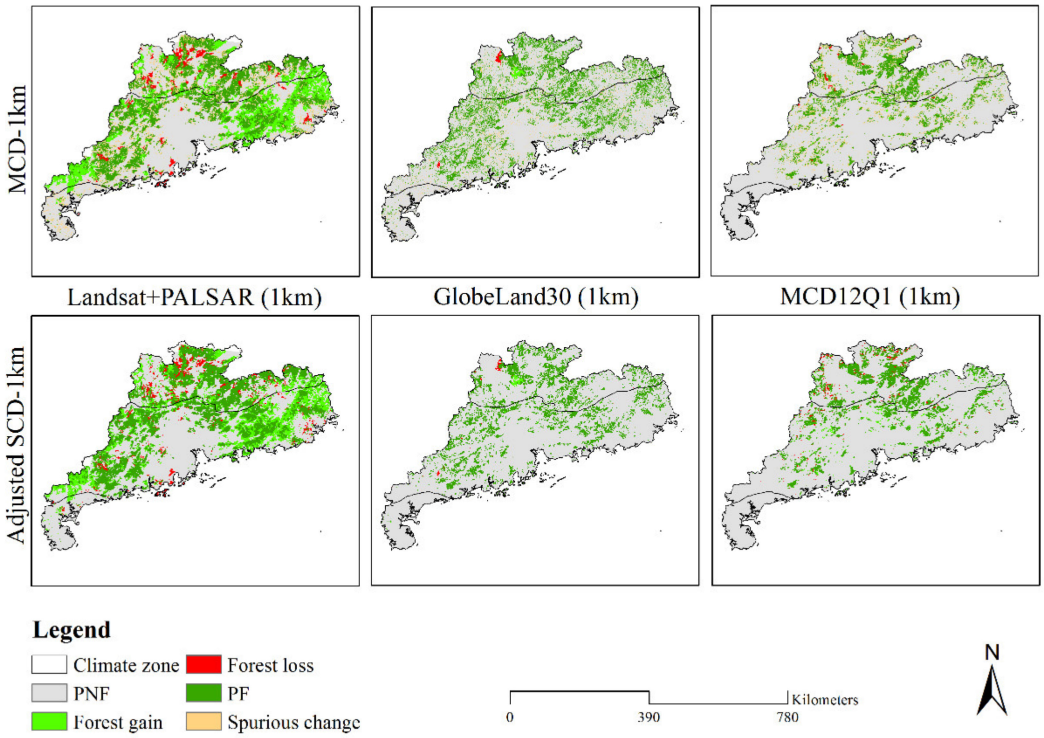

Figure 4. Change in forest cover estimated by the morphological change detection (MCD) and adjusted simple change detection (SCD) methods based on the three datasets for 30-m, 500-m, and 1-km resolutions between 2000 and 2010 showing the spatial and temporal patterns of unchanged non-forest, unchanged forest, forest gain, and forest loss in Guangdong Province, China.

Based on the forest area of the National Forestry Statistics Yearbook of China, Guangdong's forest area increased from 8.27×10^6 ha to 8.74×10^6 ha (Table 3) from 2000–2010, corresponding to a 3% increase in forest cover for the total land area of Guangdong Province. Estimates of net forest area gain ranging from 0.02–9% for 30-m resolution and 0.1–12% for 1-km resolution were observed for the three datasets; only the MODIS LC by MCD yielded net forest area losses (–0.6% for 30-m and –0.1% for 1-km). The largest net increases in forest area were found in the Landsat/PALSAR-based FNF: 9% for 30-m and 12% for 1-km.

Forest gain and loss estimates exhibited large discrepancies among the datasets in terms of both spatial pattern and total change area (Figures 4 and 5). The Landsat/PALSAR-based FNF showed a widespread change throughout the northern and northeastern Guangdong. The MODIS LC results displayed similar spatial patterns, but smaller estimated change areas of forest gain and loss when compared to those of the Landsat/PALSAR-based FNF. The GlobeLand30-based results failed to detect noticeable forest gain and loss. There was significant agreement between the no-change forest and non-forest. Agreement in forest loss with less coverage was observed in northern Guangdong. However, the numbers of highly consistent forest-gain pixels were negligibly smaller than the numbers of forest-loss pixels. Two method-based maps from the Landsat/PALSAR-based FNF for 30-m resolution and the GlobeLand30 for 1-km showed similar areas of largest and smallest forest loss, while that from the Landsat/PALSAR-based FNF based on the two methods showed similar largest forest gains for 30-m and 1-km.

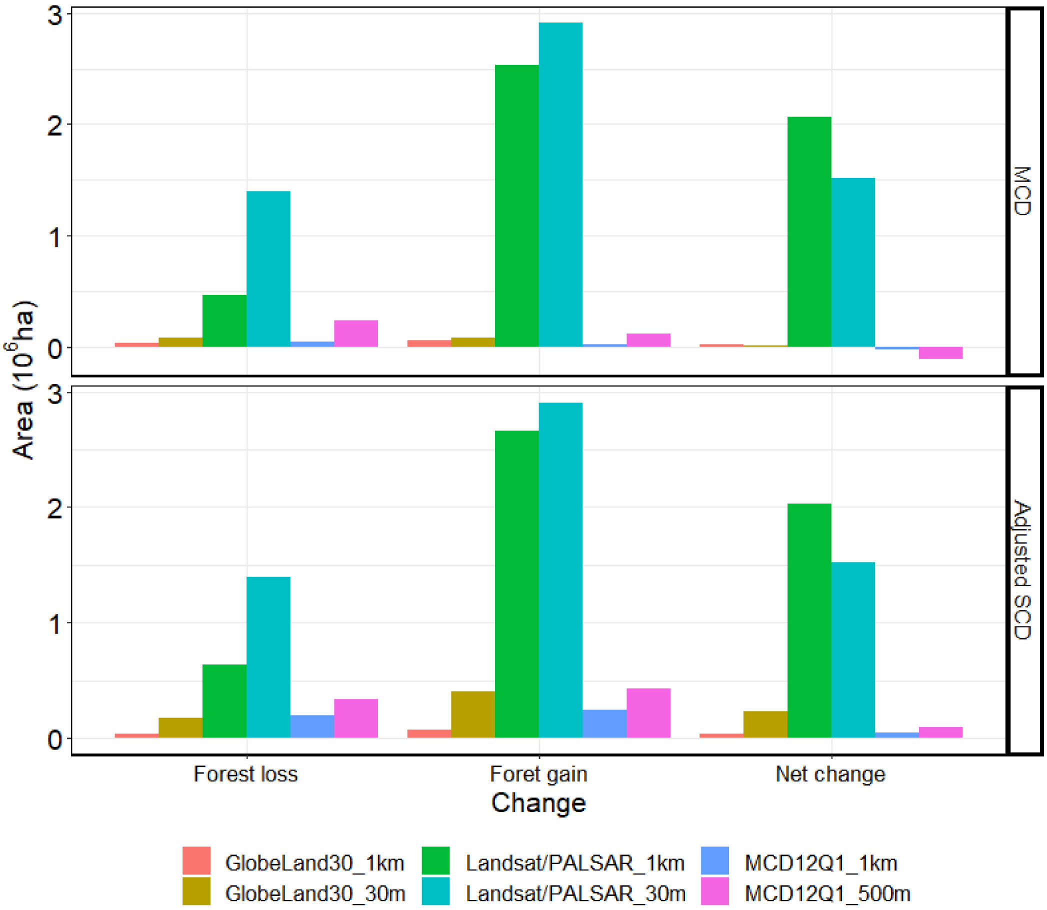

Figure 5. Areas of forest gain, loss, and net change in Guangdong, China from 2000–2010.

3.3. Spatiotemporal Impacts of Forest Cover Change on Surface Temperature

We examined the spatial distribution pattern of diurnal LST, ET, and albedo from 2000–2010 for the forest loss and gain estimates of the three datasets by the MCD and SCD methods presented in Figure 4. We focused on the forest change estimation of the Landsat/PALSAR dataset and its impact on surface temperature, since the other two datasets failed to detect most of the forest changes. We found obvious changes in annual daytime LST, nighttime LST, ET, and albedo in the forest loss and gain area mapped with the Landsat/PALSAR dataset (Figure 6). LST values, especially daytime LST, increased from 2000–2010 in forest loss areas in northern Guangdong, while increases of nighttime LST were found in forest gain areas in northeastern Guangdong. A significant LST decrease was observed in the forest gain areas, especially in southern Guangdong.

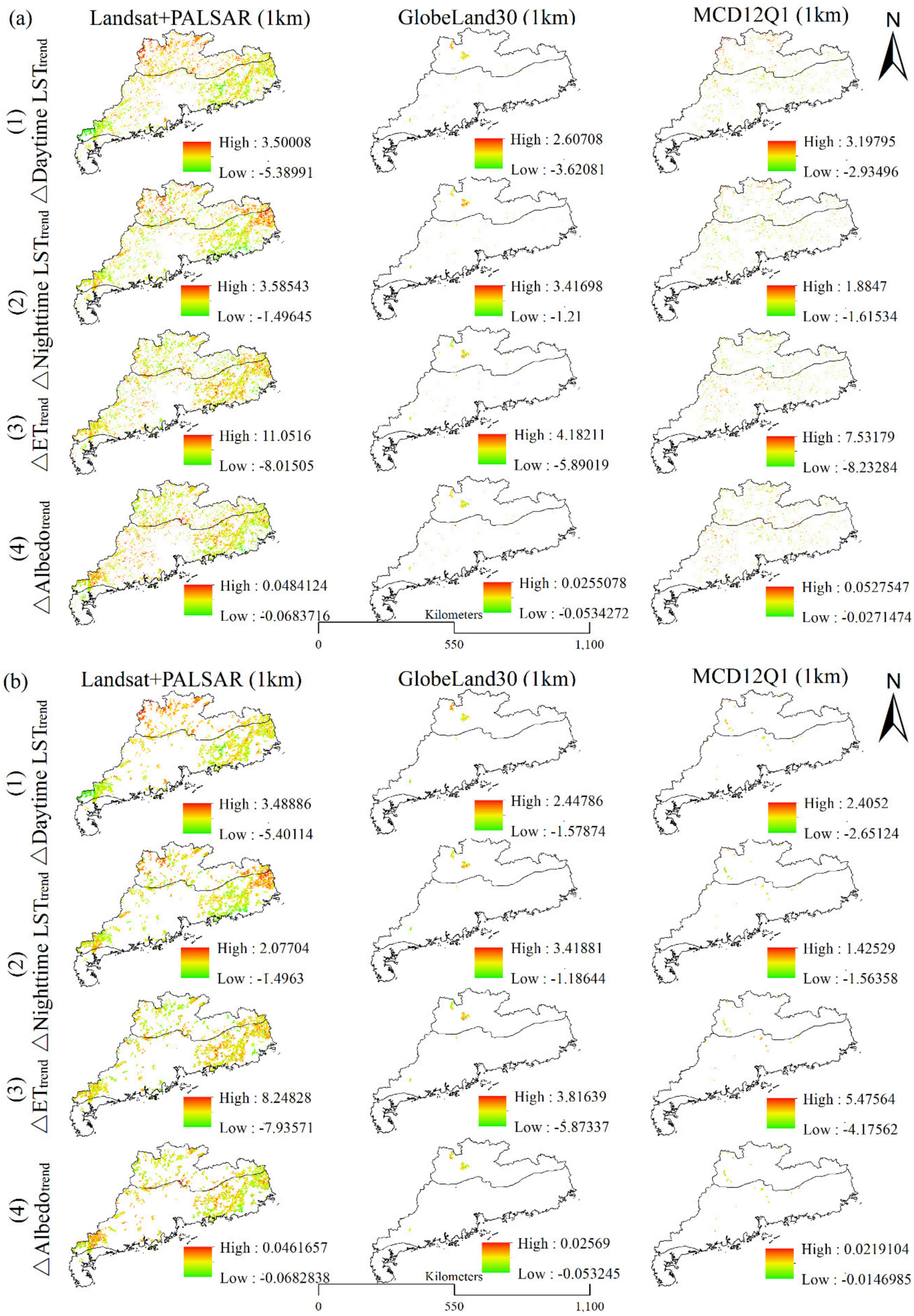

Figure 6. Changes in forest loss and gain areas at 1-km resolution from (**a**) adjusted SCD and (**b**) MCD based on the Landsat/PALSAR, GlobeLand30, and MCD12Q1 datasets (shown in Figure 4) of annual daytime LST, nighttime LST, ET, and albedo in Guangdong Province, China from 2000–2010.

3.3.1. Effects of Forest Loss and Gain on Yearly and Latitudinal Variations of LST Change

According to the Landsat/PALSAR and MCD12Q1 datasets, annual forest loss exerts consistently positive impacts on the mean land surface temperature, as generated by either the SCD or MCD methods, while forest gain exerts consistently negative effects (Figure 7). For the Landsat/PALSAR dataset, the daytime warming caused by forest loss (MCD: 0.21 ± 0.01 °C; SCD: 0.15 ± 0.01 °C) was offset by the daytime cooling caused by forest gain (MCD: −0.32 ± 0.01 °C; SCD: −0.27 ± 0.01 °C) ($P < 0.05$, Student's t test), resulting in an overall decreasing trend in daytime LST across all of Guangdong Province. The warming and cooling signs at night related to forest loss and gain were opposite those during the day, although the nighttime temperature balance between forest gain and loss can lead to less obvious cooling. Overall, there was a consistent cooling effect (MCD: −0.06 ± 0.01 °C; SCD: −0.06 ± 0.01 °C) during the day, which was greater than the nighttime effect (MCD: 0.002 ± 0.01 °C; SCD: 0.003 ± 0.01 °C). This suggests that forest gain contributed more to cooling LST (MCD: −0.15 ± 0.01 °C; SCD: −0.12 ± 0.01 °C) during both daytime and nighttime, while forest loss had a warming effect (MCD: 0.10 ± 0.01 °C; SCD: 0.07 ± 0.01 °C). Although the MODIS LC-based forest gain and loss also decreased and increased LST, respectively, during both daytime and nighttime, the overall forest cover change was associated with an increase in LST, which is opposite the Landsat/PALSAR-based results. While for the GlobeLand30-based results, increasing LST trends were found in both forest gain and loss areas.

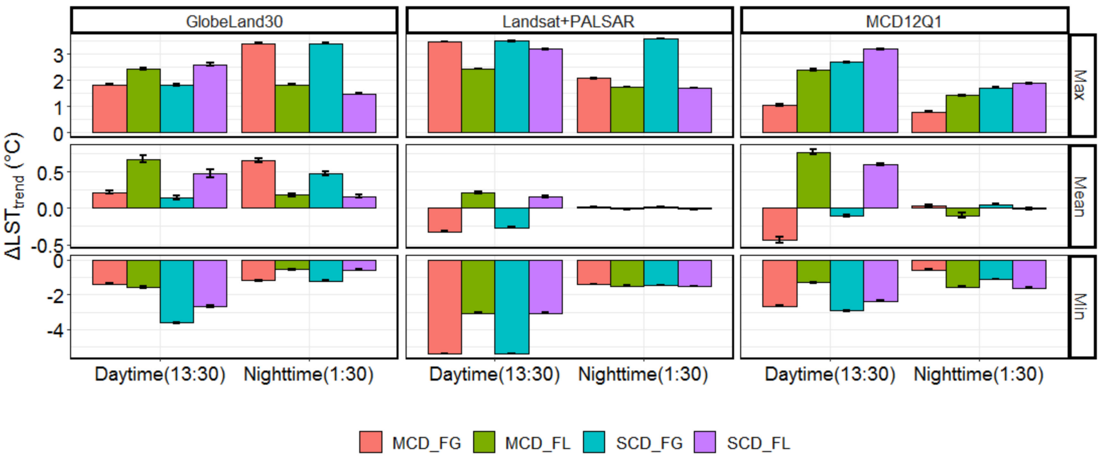

Figure 7. Annual daytime (~13:30 p.m.) and nighttime (~01:30 a.m.) LST differences caused by the three dataset-based forest loss (MCD_FL, SCD_FL) and gain (MCD_FG, SCD_FG) estimated by MCD and adjusted SCD from 2000–2010.

The magnitudes of the cooling or warming effects also varied with latitude (Figure 8). Based on the Landsat/PALSAR dataset, forest gain and loss estimated by SCD generated an LST-trend of warm to cool from the mid-subtropical to tropical zones. In particular, forest loss in the tropical zone induced the most pronounced daytime cooling effect (−0.31 ± 0.07 °C) compared to that in the south-subtropical and mid-subtropical zones (−0.10 ± 0.02 °C and 0.33 ± 0.01 °C), respectively), although less than the cooling effect from forest gain in the same zones except for the mid-subtropical zone. Moreover, forest gain and loss as determined by MCD induced warming at all latitudes, with the exception of the unusual cooling caused by forest loss (MCD: −1.44 ± 0.21 °C) in the tropical zone. Specifically, in the mid-subtropical zone, forest gain (MCD: 0.65 ± 0.01 °C; SCD: 0.30 ± 0.01 °C) and loss (MCD: 0.36 ± 0.01 °C; SCD: 0.33 ± 0.01 °C) were found to warm the daytime LST. In the other two zones, the SCD algorithm revealed that both forest gain and loss had cooling effects during the day. Likewise, at night, except in the tropical zone, all of the positive and negative signs were in agreement with those during the day, although none of them were obvious, with the exception of forest gain inducing a slight warming effect in the mid-subtropical zone.

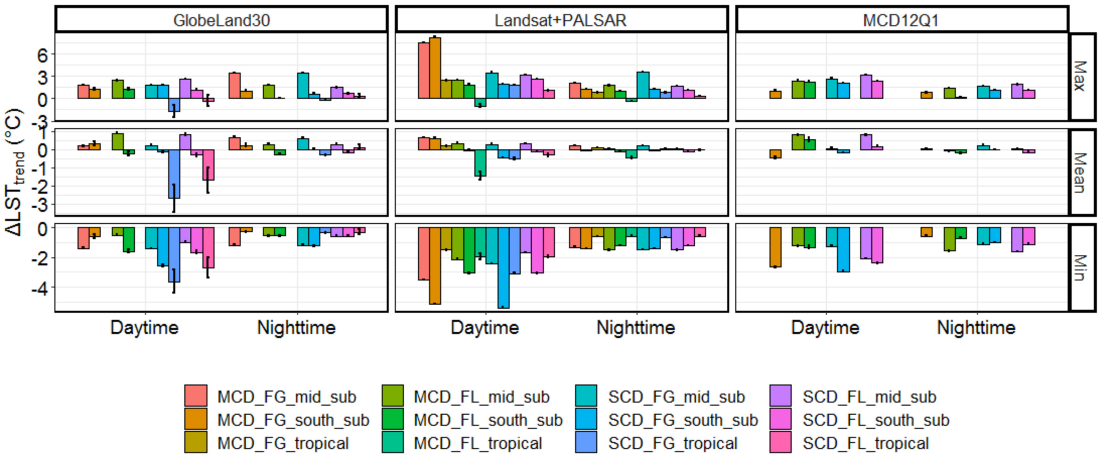

Figure 8. Annual daytime and nighttime LST differences caused by the three datasets-based forest losses and gains estimated by MCD and adjusted SCD over the mid-subtropical zone (mid_sub), south-subtropical zone (south_sub), and tropical zone (tropical) from 2000–2010. The vertical lines on each bar represent the confidence interval at 95% estimated by *t* test.

3.3.2. ET and Albedo Changes Related to Forest Loss and Gain and Their Impacts on Yearly and Latitudinal Variations of LST Change

We also summarized the trends of ET and albedo changes within forest loss and gain areas and found that all of the datasets led to similar positive and negative trends of both ET and albedo changes (Figure 9). The annual mean ET decreased due to forest loss but increased within forest gain areas. Focusing on the Landsat/PALSAR dataset, after balancing the ET trends of both forest loss and gain, the ΔET_{trend} was approximately 0.025 ± 0.01 mm per 8 d (MCD) and 0.004 ± 0.01 mm per 8 d (SCD), indicating that a total slight ET increase resulted from forest gain. Moreover, from the scatter plots (Figure S2), the ET trends associated with forest loss and gain can be roughly distinguished. The ET trend and daytime LST trend within forest gain areas exhibited negative correlations when $\Delta ET_{trend} > 0$, while within forest loss areas, both showed the same correlation when $\Delta ET_{trend} < 0$. Conversely, the ET trend displayed a positive correlation with the nighttime LST trend. The overall correlation between the ET trend and the LST trend was negative. These results revealed that there was high ET in areas with forest gain and low ET in areas with forest loss, leading to cooling and warming effects, respectively.

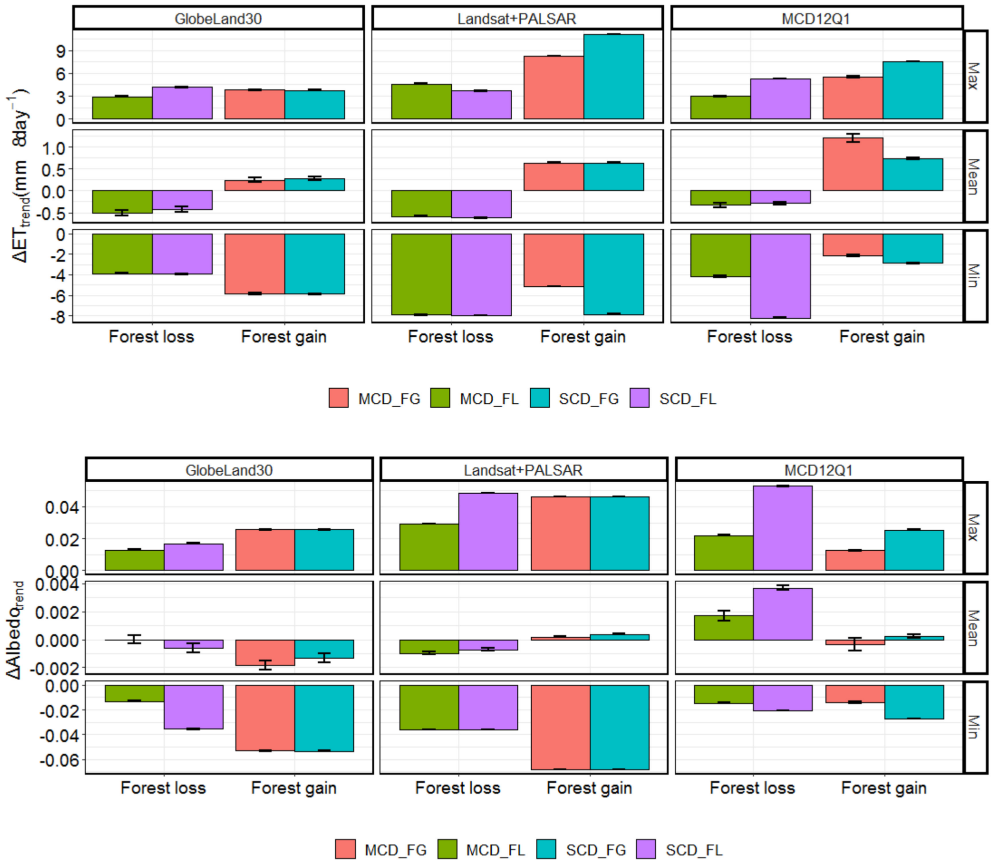

Figure 9. Annual ET and albedo differences caused by the three dataset-based forest losses and gains estimated by MCD and adjusted SCD from 2000–2010. The vertical lines on each bar represent the confidence interval at 95% estimated by *t* test.

The annual mean albedo differences between forest loss and gain areas mapped from the three datasets were inconsistent. We found both increasing and decreasing albedo within the forest gain and loss areas, which is controversial considering the fact that forests generally have low albedo [10]. Moreover, the high albedo results indicated that high land surface temperatures could not be determined by forest loss or gain (Figure S2). Thus, when compared with ET, the impacts of the interactions between albedo and LST are still not clear in the current geographical region.

For the SCD-based results, the greatest negative value (mean value < 0) of ΔET_{trend} induced by forest loss was found in the tropical zone, followed by the south-subtropical and mid-subtropical zones. Conversely, the MCD-based results identified the greatest positive value (mean value > 0) in the tropical zone (Figure 10). Meanwhile, the positive ET trend from forest gain decreased with latitude (Figure 10), although Figure S2 shows that larger positive ET values were related to lower negative LST values. An examination of these contradictory facts concerning ET in the mid-subtropical zone (Figure 10) revealed that these results indicate that the forest gain leading to LST increase was not solely induced by ET trend variations. Additionally, the forest loss-induced ET < 0 was estimated, particularly in the tropical zone. Based on the relationship in Figure S2, we found that it was a cooling effect caused by forest loss, as opposed to a warming effect (Figure 10). However, the MCD-based results showed consistent LST and ET trends in the forest loss areas (Figure 10). The SCD-based results demonstrated that forest loss in the tropical zone had a cooling effect that was unaffected by ET. The latter anomalies may be explained by the low albedo of the surface changes (Figure 10) since it was consistent with Figure S2, which indicates that low albedo could induce cooling in the tropical zone.

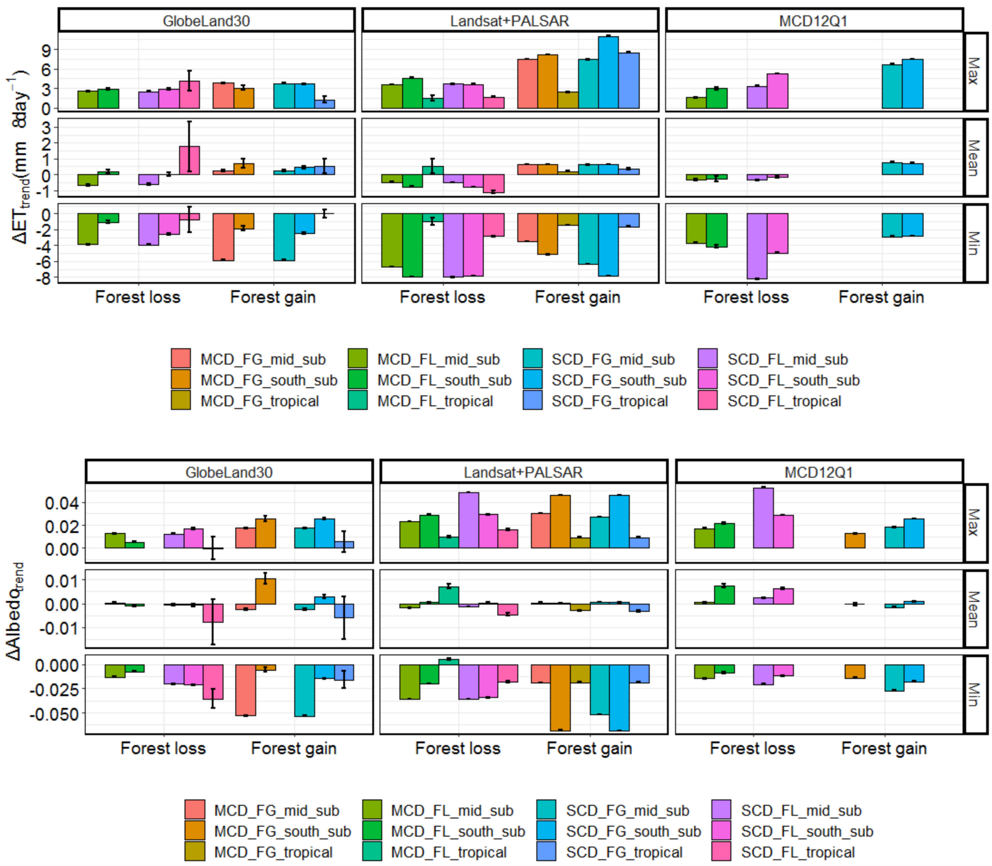

Figure 10. Annual ET and albedo differences from 2000–2010 caused by three dataset-based forest losses and gains estimated by MCD and adjusted SCD over three climate zone-based forest areas in Guangdong Province, China. The vertical lines on each bar represent the confidence interval at 95% estimated by *t* test.

3.4. Analysis of the Interrelationships about the Impacts of Forest Cover Change on Air Temperature and LST

We observed no significant positive correlations between average LST values and average air temperatures associated with forest loss and gain (Figure S3). The average LST values were generally higher than the corresponding air temperatures. It is also worth mentioning that increases in air temperature were found within the forest gain areas (MCD: 0.34 ± 0.003 °C; SCD: 0.31 ± 0.003 °C) according to the Landsat/PALSAR dataset (Figure S4). That is, forest gain had a warming effect on the air temperature, while the effect of forest loss was just opposite, leading to cooling (MCD: −0.08 ± 0.01 °C; SCD: −0.07 ± 0.01 °C) (Figure 11 and Figure S4). This conclusion is contrary to their impacts on the land surface temperature (Figures 7 and 11). Nevertheless, for the Landsat/PALSAR and MCD12Q1 datasets, the nighttime temperature differences between the two temperature datasets associated with forest loss and gain were slightly smaller than the daytime differences. In particular, the smallest average difference occurred in forest loss from the Landsat/PALSAR dataset. Using the GlobeLand30, we detected large differences between the two temperature datasets. Specifically, the temperatures in the forest gain areas exhibited larger differences than those in the forest loss areas.

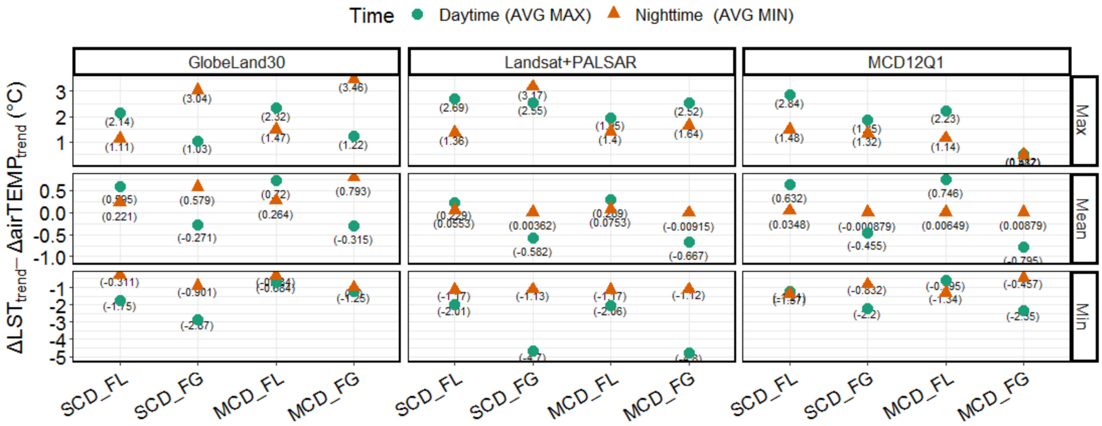

Figure 11. Differences between annual ΔLST_{trend} and $\Delta airTEMP_{trend}$ (daytime AVG MAX, nighttime AVG MIN) caused by the three dataset-based forest losses (SCD_FL, MCD_FL) and gains (SCD_FG, MCD_FG) estimated by MCD and adjusted SCD in Guangdong Province, China from 2000–2010.

4. Discussion

4.1. The Importance of Pre-Assessment Method in Forest Cover Change

This study examined the forest cover change patterns in Guangdong Province, China, from different perspectives. We have identified large inconsistencies among both remote sensing-based and NFI-based forest changes, which can be explained by the different forest definitions and resolutions among the Landsat/PALSAR, MODIS, and Landsat-based datasets. Our results also described the spatial heterogeneity of forest cover distribution and change across the study area. Our findings are consistent with those of previous studies comparing multiple datasets, such as Global Forest Change (GFC), MODIS NBR-based estimate, MODIS LC, and vegetation continuous fields (VCF) products, as well as the Landsat-based GFC [48–50]. We detected an overall forest cover increase in Guangdong based on the Landsat/PALSAR forest/non-forest and MODIS LC products, although the latter exhibited a significantly smaller increase due to the missed identifications (Figure 4). Therefore, we questioned the suitability of using the MODIS-based land cover products, either individually or for further studies at local or even global scales due to their low local accuracy, although many other studies have demonstrated the benefits of using these datasets [51,52]. Prevedello et al. [18] used two dates of Hansen's Global Forest Cover datasets [27] to evaluate the impacts of forest change on climate, suggesting that high-resolution forest maps are preferred because they can adequately capture the biophysical processes of the region of interest (forest cover), even when combined with 0.05° MODIS land surface products. Comparing maps describing changes over time should definitely not be made on the basis of past studies [53,54] due to the problematic inaccuracies inherent in the different thematic classes [29,48]. Since each study has its specific purpose, such as vegetation mapping, climate simulation, and global change response [31,52,55], developing the user-defined mapping algorithms and rules, if possible, would inevitably yield more precise monitoring.

Scaling issues also exist in the integration and application of multi-source remote sensing datasets [29,56]. We used the bilinear interpolation algorithm to resample and aggregate higher spatial resolutions to 1-km and found consistent results, with the exception of those from the GlobeLand30, although the accuracy decreased with image resolution. Other resampling methods, including cubic, nearest neighbor, and majority techniques, have been applied in forest cover scaling for the detection of forest cover change [49]. Different scaling methods can lead to noticeable impacts on the change detection results, which may explain the unusual loss area in our GlobeLand30 results.

Our derivation of forest cover change from the overlay of classified forest cover maps between different periods, along with filters and morphological operations by MCD and adjusted SCD, is also superior to the traditional two-date overlay approach [57,58], since this traditional approach will inevitably lead to classification errors due to the misregistration of maps and mixed pixels. The design of both methods aims to overcome the above deficiencies; in particular, MCD improves the change detection accuracy compared to the traditional SCD [38], although MCD uses post-processing, and the generation of spurious change does not fall into any forest cover change type (change versus no change). This spurious change type, however, does not belong to any type that would limit the evaluation of the relationship between forest change/non-change and temperature (Figures 4 and 8) [19]. Actually, in terms of accuracy, the adjusted SCD algorithm performed better than the MCD when mapping forest change. In addition, although post-classification comparison analysis is a popular method [59], the accuracy of the individual classification results would determine the change detection accuracy [33]. We found, however, that even when the two classifications were accurate, the accuracy of the change map was low, especially for forest loss and gain, which could then have led to errors in the calculation of the area (Tables S1 and S2). Indeed, these key points should be taken seriously since they will affect the accurate determination of forest change and its impacts.

4.2. Evaluation of the Impacts of Forest Change on Temperature

Forest loss and gain, also known as deforestation and afforestation [15,18], have been found to be widespread at a regional scale in Guangdong, China, and were discovered to exert strong and opposing effects on local LST, ET, and albedo [15,18]. Specifically, forest gain showed the potential to reverse the effect of forest loss on LST and ET, although not on albedo, suggesting the importance of reducing deforestation and increasing afforestation. Although deforestation can increase albedo and forestation can decrease albedo globally [18], we found the effects of forest gain and loss on LST are more influenced by ET than by albedo, most likely because snow-feedback-based albedo is usually less effective at lower latitudes [60].

These findings reflect the results from the Landsat/PALSAR-based forest change dataset, since the performances of the other two datasets were relatively poor at the regional scale. Using the forest change data based on a coarse spatial resolution could be inaccurate due to the lack of spatial details [61]. Many studies have advocated the use of MODIS-based data, drawing consistent conclusions about the relationships between forest change and climate [16,23–25]. Although their findings can be acceptable, the magnitude of the impacts may not be guaranteed. Based on the Landsat/PALSAR data, we detected an overall cooling effect induced by forest gain and loss. The MODIS-based results, however, demonstrated the opposite effects. This proves that the impacts of land cover change on climate conditions obtained with MODIS data on the global scale are not transferrable to the regional scale. Thus, high-resolution maps are suitable for the evaluation of climate response to forest change [18].

The relationships between forest cover change and surface temperature also exhibited strong spatial heterogeneity across latitudes. We found that forest gain had a strong warming effect on local LST in the mid-subtropical zone. This could be explained by the replacement of natural forests with planted forests north of 24°N in Guangdong Province [26]. Moreover, warming was not mediated by ET, because increasing ET led to cooling. The low albedo of afforested areas with dark leaves led to a warming effect, and the ET cooling constrained by the dry climate led to the increasing warming due to forest gain in northern Guangdong [26,62]. The decrease of ET due to forest loss led to a warming effect, albeit with a decreasing trend, because the temperatures related to the nearby land types were lower than the temperatures induced by the forest changes (Figure S5). In addition, we confirmed that there was reduced warming due to forest gain as well as forest loss across latitudes. We demonstrated that current land use policies are likely to exert impacts on the local climate [18]. We found a forest loss-induced cooling effect in the tropical zone (20°N–21°30′N), although it was relatively rare. Warming in the tropical regions due to deforestation is a common conclusion [10,63]. Historically, the Leizhou Peninsula developed short-cycle industrial raw material forests, especially monoculture eucalyptus forests, after the reduction of large-scale tropical monsoon forests. Planted forests such as eucalyptus have been removed as part of the cutting rotation. However, the cooling from a lower surface albedo as well as the continuing irrigation of dry farmland based on the Yearbook of Guangdong Agriculture and Countryside can limit the increasing warming and actually lead to a cooling effect [64,65]. While the enhanced cooling caused by forest gain contributed more during ET, it was constrained by the nearby bare red soil that was depleted of soil moisture (Figure S5) [66]. Moreover, the forest gain from rain-fed farmland observed in western Guangdong led to a cooling effect [26], and the surrounding irrigated farmland also contributed a slightly cooling benefit, resulting in an overall cooling in the south-subtropical zone. Meanwhile, less obvious cooling in this region was found as a result of forest cutting due to cooling in the change area itself from the irrigated farmland (Figure S5).

Generally, the reduced surrounding temperatures related to nearby land cover types varied with latitude (Figure S5). These kinds of local differences did not increase the temperatures in the tropical zone, nor decreased temperatures in the northern latitude region, however, and either decreased temperature in the south and increased temperature in the north, or at least dampened the temperature decrease and rise (Figure 8 and Figure S5). For example, in the tropical forest zone, the nearby temperature decrease due to forest loss was to the result of shortwave radiation and moisture stress associated with a dry climate [23]. This finding agreed with the climate model-based study concerning tropical deforestation in the Sahel and other regions [67]. Climate change induced by other local no-change types is an important factor, but the specific causes of this change may determine the magnitude to which temperature is affected. Prevedello et al. [18] found native and planted forests affect local climate, but Hansen's Global Land Change dataset cannot include these types. Unfortunately, none of the three datasets in this study distinguished rain-fed farmland from either irrigated farmland, as well as bare soil, which may limit the spatial quantitative explanation. Despite this limitation, however, high-resolution maps, combined with recent studies [26,34,37], help us to better understand how the biophysical mechanisms of actual forest changes impact climate.

After considering the effect of the surrounding land cover types, our study found that the magnitude of reduced warming due to afforestation varied with latitude. Ge et al. [24] reported a non-radiative cooling effect from afforestation on local LST in China, and concluded that the effect of background temperature cannot be ignored, since it can influence the impacts of forest change on climate by altering biophysical processes via atmospheric feedback [19]. It should be noted that these feedbacks from either afforestation or deforestation have been considered in climate models in order to enhance the simulation performance [7,19]. Since our study only utilized the satellite observation-based method without climate simulation, the impacts of deforestation on climate are unlike the results based on the Earth system model [67]. These regional climate differences may not be reflected in observations. Moreover, we discovered huge discrepancies between LST and air temperature. We believe that a possible explanation for this is that there is a spurious signal due to an inconspicuous spatially interpolated air temperatures response to forest change (Figures S4 and S5). It also shows that forest change feedback on surface temperature is more reliable. Hence, the results of the many studies that did not consider the nearby background temperatures and detailed forest change types are uncertain, even if the background effects were not readily apparent.

In summary, the local effects of forest change on LST in Guangdong Province, China are primarily modulated by ET, while the latitude variations are modulated by both ET and albedo, even though the effect of albedo is negligible at this latitude.

4.3. Limitations and Insights of This Study

Uncertainties exist in our estimation of forest cover change in Guangdong, China. The sample size of the spatial change can affect the response of surface temperature to biophysical changes associated with land cover change [68]. The moving-window sampling method, which can verify the pixel-based and land cover type-based accuracies, can be used to support future studies [25]. Our method needs to ensure pixel quality at a large scale as well as the accuracy of the climate response by improving the change detection results. Additionally, some specific land use types, particularly those influenced by local economies and policies, can cause temperature differences that differ from those of other global or regional studies. Moreover, in this work, we simply quantified the forest change patterns with existing datasets. Future efforts are required to understand the driving forces behind forest change in Guangdong Province.

High-quality monitoring of forest changes can be used to reveal many subtle variations which can then help us understand their actual impacts on climate [18]. This monitoring will play a new role in combination with climate models (e.g., global or regional) and site observations (e.g., flux tower or weather station) to simulate climate change, especially when precipitation, cloud, soil moisture, LAI, and latent heat flux, and sensible heat flux are taken into account. It is no wonder that the accuracy of global scale datasets is low at the local scale. Although many studies have concluded that it would be too arbitrary to determine which dataset is more suitable for a specific application [48,53], our study not only provides a reference for users in the same field, but also emphasizes the importance of developing highly accurate data at the local scale in order to provide a practical and effective basis for revealing the response of forest change to climate change through satellite observations in planted forest areas or similar geographical regions.

5. Conclusions

In this study, we developed three forest change products for Guangdong Province, China using different forest cover datasets, and evaluated the impacts of forest loss and gain on surface temperature using pixel-based spatiotemporal change pattern methods based on these products. Specifically, we used the adjusted SCD and MCD algorithms to detect forest change and validated the datasets at the spatial resolution of 30-m and 1-km. We discovered that even if the accuracy of an individual forest cover dataset is high, the change detection accuracy could decrease, and there may be errors due to limited samples in the reference data used to validate the forest change. The large discrepancies among these datasets would then affect the derived contribution of forest change to LST.

Here, we chose the relatively optimal Landsat/PALSAR-based forest changes as an example for further analysis. We discovered that forest loss and gain induced annual increasing and decreasing trends of LST, respectively, while forest change exerted an overall cooling effect on LST in Guangdong. These changes were predominantly modulated by ET cooling and surrounding temperatures. However, the presence of these factors, such as the ET cooling induced by forest gain in the mid-subtropical zone constrained by dry conditions and warming induced by forest loss in the tropical zone limited by irrigated farmland, led to the opposite temperature changes. Although challenges still exist for identifying the drivers of forest change and evaluating their impacts on temperature, high-resolution forest change maps were found to be preferable for monitoring the impacts of forests on climate. Overall, our analysis revealed that forest gain has the potential to reverse the climate effects of forest loss. It is suggested that positive climate feedback can be achieved through the reasonable regulation of forest loss and gain. For example, forest gain should be carried out in areas where forest once existed in order to help improve biodiversity and avoid further impacts of land cover change on the local climate.

Supplementary Materials: The following are available online at http://www.mdpi.com/2072-4292/12/15/2354/s1, Figure S1, Figure S2, Figure S3, Figure S4, Figure S5, Table S1, Table S2, Table S3.

Author Contributions: W.S. designed the study, analyzed the data, and wrote the paper. M.L. and C.H. helped in project design and analysis. J.H. helped in paper review and editing. All authors have read and agreed to the published version of the manuscript.

Funding: This work was jointly supported by the Natural Science Foundation of China [31971577], China Postdoctoral Science Foundation [2019M651842], and the Priority Academic Program Development of Jiangsu Higher Education Institutions (PAPD). Additionally, this work was performed while the first author was funded by the 2019 Postdoctoral Fellowships of Jiangsu Province.

Acknowledgments: The anonymous reviewers' comments and suggestions greatly improved our paper. We are grateful for their kind help. Special thanks need to go to the Land Processes Distributed Active Archive Center, they provided the MODIS data. The authors also thank the Guangdong Provincial Center for Forest Resources Monitoring for providing field inventories, Yan Li in Beijing Normal University, China in provision of the aid of methods interpretation, and Hao Jiang in Guangzhou Institute of Geography, Guangdong Academy of Sciences, China in assisting in the identification of local land cover types.

Conflicts of Interest: No potential conflict of interest was reported by the authors.

References

1. Bathiany, S.; Claussen, M.; Brovkin, V.; Raddatz, T.; Gayler, V. Combined biogeophysical and biogeochemical effects of large-scale forest cover changes in the MPI earth system model. *Biogeosciences* **2010**, *7*, 1383–1399. [CrossRef]
2. Bonan, G.B. Forests and climate change forcings, feedbacks, and the climate benefits of forests. *Science* **2008**, *320*, 1444–1449. [CrossRef] [PubMed]
3. Bright, R.M.; Davin, E.; O'Halloran, T.; Pongratz, J.; Zhao, K.; Cescatti, A. Local temperature response to land cover and management change driven by non-radiative processes. *Nat. Clim. Change* **2017**, *7*, 296–302. [CrossRef]
4. Chase, T.N.; Pielke, R.A., Sr.; Kittel, T.G.F.; Nemani, R.R.; Running, S.W. Simulated impacts of historical land cover changes on global climate in northern winter. *Clim. Dyn.* **2000**, *16*, 93–105. [CrossRef]
5. Zhao, K.; Jackson, R. Biophysical forcings of land-use changes from potential forestry activities in North America. *Ecol. Monogr.* **2014**, *84*, 329–353. [CrossRef]
6. Burakowski, E.; Tawfik, A.; Ouimette, A.; Lepine, L.; Novick, K.; Ollinger, S.; Zarzycki, C.; Bonan, G. The role of surface roughness, albedo, and Bowen ratio on ecosystem energy balance in the Eastern United States. *Agric. For. Meteorol.* **2018**, *249*, 367–376. [CrossRef]
7. Chen, L.; Dirmeyer, P.A. Reconciling the disagreement between observed and simulated temperature responses to deforestation. *Nat. Commun.* **2020**, *11*, 202. [CrossRef]
8. Huang, B.; Hu, X.; Fuglstad, G.A.; Zhou, X.; Zhao, W.; Cherubini, F. Predominant regional biophysical cooling from recent land cover changes in Europe. *Nat. Commun.* **2020**, *11*, 1–13. [CrossRef]
9. Li, Z.; Tang, B.; Wu, H.; Ren, H.; Yan, G.; Wan, Z.; Trigo, I.F.; Sobrino, J.A. Satellite-derived land surface temperature: Current status and perspectives. *Remote Sens. Environ.* **2013**, *131*, 14–37. [CrossRef]
10. Alkama, R.; Cescatti, A. Biophysical climate impacts of recent changes in global forest cover. *Science* **2016**, *351*, 600–604. [CrossRef]
11. Lee, X.; Goulden, M.L.; Hollinger, D.Y.; Barr, A.; Black, T.A.; Bohrer, G.; Bracho, R.; Drake, B.; Goldstein, A.; Gu, L.; et al. Observed increase in local cooling effect of deforestation at higher latitudes. *Nature* **2011**, *479*, 384–387. [CrossRef] [PubMed]
12. Senior, R.A.; Hill, J.K.; Gonzalez Del Pliego, P.; Goode, L.K.; Edwards, D.P. A pantropical analysis of the impacts of forest degradation and conversion on local temperature. *Ecol. Evol.* **2017**, *7*, 7897–7908. [CrossRef] [PubMed]
13. Strandberg, G.; Kjellström, E. Climate impacts from afforestation and deforestation in Europe. *Earth Interact.* **2019**, *23*, 1–27. [CrossRef]
14. Wang, L.; Lee, X.; Schultz, N.; Chen, S.; Wei, Z.; Fu, C.; Gao, Y.; Yang, Y.; Lin, G. Response of surface temperature to afforestation in the Kubuqi Desert, Inner Mongolia. *J. Geophys. Res. Atmos.* **2018**, *123*, 948–964. [CrossRef]
15. Li, Y.; Zhao, M.; Mildrexler, D.J.; Motesharrei, S.; Mu, Q.; Kalnay, E.; Zhao, F.; Li, S.; Wang, K. Potential and Actual impacts of deforestation and afforestation on land surface temperature. *J. Geophys. Res. Atmos.* **2016**, *121*, 14372–14386. [CrossRef]
16. Peng, S.S.; Piao, S.; Zeng, Z.; Ciais, P.; Zhou, L.; Li, L.Z.; Myneni, R.B.; Yin, Y.; Zeng, H. Afforestation in China cools local land surface temperature. *Proc. Natl. Acad. Sci. USA* **2014**, *111*, 2915–2919. [CrossRef]
17. Perugini, L.; Caporaso, L.; Marconi, S.; Cescatti, A.; Quesada, B.; de Noblet-Ducoudré, N.; House, J.I.; Arneth, A. Biophysical effects on temperature and precipitation due to land cover change. *Environ. Res. Lett.* **2017**, *12*, 053002. [CrossRef]
18. Prevedello, J.A.; Winck, G.R.; Weber, M.M.; Nichols, E.; Sinervo, B. Impacts of forestation and deforestation on local temperature across the globe. *PLoS ONE* **2019**, *14*, e0213368. [CrossRef]
19. Devaraju, N.; de Noblet-Ducoudré, N.; Quesada, B.; Bala, G. Quantifying the relative importance of direct and indirect biophysical effects of deforestation on surface temperature and teleconnections. *J. Clim.* **2018**, *31*, 3811–3829. [CrossRef]

20. Duveiller, G.; Forzieri, G.; Robertson, E.; Li, W.; Georgievski, G.; Lawrence, P.; Wiltshire, A.; Ciais, P.; Pongratz, J.; Sitch, S.; et al. Biophysics and vegetation cover change: A process-based evaluation framework for confronting land surface models with satellite observations. *Earth Syst. Sci. Data* **2018**, *10*, 1265–1279. [CrossRef]
21. MacDougall, A.H.; Beltrami, H. Impact of deforestation on subsurface temperature profiles: Implications for the borehole paleoclimate record. *Environ. Res. Lett.* **2017**, *12*, 074014. [CrossRef]
22. Anderson, R.G.; Canadell, J.G.; Randerson, J.T.; Jackson, R.B.; Hungate, B.A.; Baldocchi, D.D.; Ban-Weiss, G.A.; Bonan, G.B.; Caldeira, K.; Cao, L.; et al. Biophysical considerations in forestry for climate protection. *Front. Ecol. Environ.* **2011**, *9*, 174–182. [CrossRef]
23. Tang, B.; Zhao, X.; Zhao, W. Local effects of forests on temperatures across Europe. *Remote Sens.* **2018**, *10*, 529. [CrossRef]
24. Ge, J.; Guo, W.; Pitman, A.J.; De Kauwe, M.G.; Chen, X.; Fu, C. The nonradiative effect dominates local surface temperature change caused by afforestation in China. *J. Clim.* **2019**, *32*, 4445–4471. [CrossRef]
25. Li, Y.; Zhao, M.; Motesharrei, S.; Mu, Q.; Kalnay, E.; Li, S. Local cooling and warming effects of forests based on satellite observations. *Nat. Commun.* **2015**, *6*, 6603. [CrossRef] [PubMed]
26. Shen, W.; Li, M.; Huang, C.; He, T.; Tao, X.; Wei, A. Local land surface temperature change induced by afforestation based on satellite observations in Guangdong plantation forests in China. *Agric. For. Meteorol.* **2019**, *276–277*, 107641. [CrossRef]
27. Hansen, M.C.; Potapov, P.V.; Moore, R.; Hancher, M.; Turubanova, S.A.; Tyukavina, A.; Thau, D.; Stehman, S.V.; Goetz, S.J.; Loveland, T.R.; et al. High-resolution global maps of 21st-century forest cover change. *Science* **2013**, *342*, 850–853. [CrossRef]
28. Pitman, A.J.; Avila, F.B.; Abramowitz, G.; Wang, Y.P.; Phipps, S.J.; de Noblet-Ducoudre, N. Importance of background climate in determining impact of land-cover change on regional climate. *Nat. Clim. Change* **2011**, *1*, 472–475. [CrossRef]
29. Novo-Fernández, A.; Franks, S.; Wehenkel, C.; López-Serrano, P.M.; Molinier, M.; López-Sánchez, C.A. Landsat time series analysis for temperate forest cover change detection in the Sierra Madre Occidental, Durango, Mexico. *Int. J. Appl. Earth Obs. Geoinf.* **2018**, *73*, 230–244. [CrossRef]
30. Wickham, J.D.; Wade, T.G.; Riitters, K.H. Empirical analysis of the influence of forest extent on annual and seasonal surface temperatures for the continental United States. *Global Ecol. Biogeogr.* **2013**, *22*, 620–629. [CrossRef]
31. Liang, S.; Wang, J. Chapter 25—Forest Cover Changes: Mapping and Climatic Impact Assessment. In *Advanced Remote Sensing*; Academic Press: Cambridge, MA, USA, 2020; pp. 915–952. [CrossRef]
32. Olofsson, P.; Foody, G.M.; Herold, M.; Stehman, S.V.; Woodcock, C.E.; Wulder, M.A. Good practices for estimating area and assessing accuracy of land change. *Remote Sens. Environ.* **2014**, *148*, 42–57. [CrossRef]
33. Olofsson, P.; Foody, G.M.; Stehman, S.V.; Woodcock, C.E. Making better use of accuracy data in land change studies: Estimating accuracy and area and quantifying uncertainty using stratified estimation. *Remote Sens. Environ.* **2013**, *129*, 122–131. [CrossRef]
34. Chen, J.; Chen, J.; Liao, A.; Cao, X.; Chen, L.; Chen, X.; He, C.; Han, G.; Peng, S.; Lu, M.; et al. Global land cover mapping at 30m resolution: A POK-based operational approach. *ISPRS J. Photogramm.* **2015**, *103*, 7–27. [CrossRef]
35. Shimada, M.; Itoh, T.; Motooka, T.; Watanabe, M.; Shiraishi, T.; Thapa, R.; Lucas, R. New global forest/non-forest maps from ALOS PALSAR data (2007–2010). *Remote Sens. Environ.* **2014**, *155*, 13–31. [CrossRef]
36. Shen, W.; Li, M.; Huang, C.; Tao, X.; Li, S.; Wei, A. Mapping annual forest change due to afforestation in Guangdong province of China using active and passive remote sensing data. *Remote Sens.* **2019**, *11*, 490. [CrossRef]
37. Sulla-Menashe, D.; Gray, J.M.; Abercrombie, S.P.; Friedl, M.A. Hierarchical mapping of annual global land cover 2001 to present: The MODIS Collection 6 Land Cover product. *Remote Sens. Environ.* **2019**, *222*, 183–194. [CrossRef]
38. Seebach, L.; Strobl, P.; Vogt, P.; Mehl, W.; San-Miguel-Ayanz, J. Enhancing post-classification change detection through morphological post-processing—A sensitivity analysis. *Int. J. Remote Sens.* **2013**, *34*, 7145–7162. [CrossRef]

39. Thomas, N.E.; Huang, C.Q.; Goward, S.N.; Powell, S.; Schleeweis, K.; Hinds, A. Validation of North American forest disturbance dynamics derived from Landsat time series stacks. *Remote Sens. Environ.* **2011**, *115*, 19–32. [CrossRef]
40. Lei, X.D.; Tang, M.P.; Lu, Y.C.; Hong, L.X.; Tian, D.L. Forest inventory in China: Status and challenges. *Int. For. Rev.* **2009**, *11*, 52–63. [CrossRef]
41. Huang, C.Q.; Coward, S.N.; Masek, J.G.; Thomas, N.; Zhu, Z.L.; Vogelmann, J.E. An automated approach for reconstructing recent forest disturbance history using dense Landsat time series stacks. *Remote Sens. Environ.* **2010**, *114*, 183–198. [CrossRef]
42. Shen, W.J.; Li, M.S.; Wei, A.S. Spatio-temporal variations in plantation forests disturbance and recovery of Northern Guangdong Province using yearly Landsat time series observations (1986–2015). *Chin. Geogr. Sci.* **2017**, *27*, 600–613. [CrossRef]
43. Huang, C.; Davis, L.S.; Townshend, J.R.G. An assessment of support vector machines for land cover classification. *Int. J. Remote Sens.* **2002**, *23*, 725–749. [CrossRef]
44. Wan, Z. New refinements and validation of the MODIS Land-Surface Temperature/Emissivity products. *Remote Sens. Environ.* **2008**, *112*, 59–74. [CrossRef]
45. Mu, Q.Z.; Zhao, M.S.; Running, S.W. Improvements to a MODIS global terrestrial evapotranspiration algorithm. *Remote Sens. Environ.* **2011**, *115*, 1781–1800. [CrossRef]
46. Schaaf, C.B.; Gao, F.; Strahler, A.H.; Lucht, W.; Li, X.; Tsang, T.; Lewis, P. First operational BRDF, albedo nadir reflectance products from MODIS. *Remote Sens. Environ.* **2002**, *83*, 135–148. [CrossRef]
47. Mildrexler, D.J.; Zhao, M.; Running, S.W. A global comparison between station air temperatures and MODIS land surface temperatures reveals the cooling role of forests. *J. Geophys. Res.* **2011**, *116*. [CrossRef]
48. Bai, Y.; Feng, M.; Jiang, H.; Wang, J.; Zhu, Y.; Liu, Y. Assessing consistency of five global land cover data sets in China. *Remote Sens.* **2014**, *6*, 8739–8759. [CrossRef]
49. Li, Y.; Sulla-Menashe, D.; Motesharrei, S.; Song, X.P.; Kalnay, E.; Ying, Q.; Li, S.; Ma, Z. Inconsistent estimates of forest cover change in China between 2000 and 2013 from multiple datasets: Differences in parameters, spatial resolution, and definitions. *Sci. Rep.* **2017**, *7*, 8748. [CrossRef]
50. Pérez-Hoyos, A.; García-Haro, F.J.; San-Miguel-Ayanz, J. Conventional and fuzzy comparisons of large scale land cover products: Application to CORINE, GLC2000, MODIS and GlobCover in Europe. *ISPRS J. Photogramm.* **2012**, *74*, 185–201. [CrossRef]
51. Wessels, K. Mapping regional land cover with MODIS data for biological conservation: Examples from the Greater Yellowstone Ecosystem, USA and Para State, Brazil. *Remote Sens. Environ.* **2004**, *92*, 67–83. [CrossRef]
52. Wulder, M.A.; Coops, N.C.; Roy, D.P.; White, J.C.; Hermosilla, T. Land cover 2.0. *Int. J. Remote Sens.* **2018**, *39*, 4254–4284. [CrossRef]
53. Gebhardt, S.; Wehrmann, T.; Ruiz, M.A.M.; Maeda, P.; Bishop, J.; Schramm, M.; Kopeinig, R.; Cartus, O.; Kellndorfer, J.; Ressl, R.; et al. MAD-MEX: Automatic wall-to-wall land cover monitoring for the Mexican REDD-MRV program using all Landsat data. *Remote Sens.* **2014**, *6*, 3923–3943. [CrossRef]
54. Homer, C.; Dewitz, J.; Fry, J.; Coan, M.; Hossain, N.; Larson, C.; Herold, N.; McKerrow, A.; VanDriel, J.N.; Wickham, J. Completion of the 2001 national land cover database for the counterminous United States. *Photogramm. Eng. Remote Sens.* **2007**, *73*, 337.
55. Duveiller, G.; Hooker, J.; Cescatti, A. The mark of vegetation change on Earth's surface energy balance. *Nat. Commun.* **2018**, *9*, 679. [CrossRef] [PubMed]
56. Quattrochi, D.A.; Wentz, E.; Lam, N.S.-N.; Emerson, C.W. *Integrating Scale in Remote Sensing and GIS*; CRC Press: Boca Raton, FL, USA, 2017.
57. Foody, G.M. Harshness in image classification accuracy assessment. *Int. J. Remote Sens.* **2008**, *29*, 3137–3158. [CrossRef]
58. Serra, P.; Pons, X.; Saurí, D. Post-classification change detection with data from different sensors: Some accuracy considerations. *Int. J. Remote Sens.* **2003**, *24*, 3311–3340. [CrossRef]
59. Singh, A. Review article digital change detection techniques using remotely-sensed data. *Int. J. Remote Sens.* **1989**, *10*, 989–1003. [CrossRef]
60. Hall, A. The role of surface albedo feedback in Climate. *J. Clim.* **2004**, *17*, 1550–1568. [CrossRef]
61. Townshend, J.R.; Masek, J.G.; Huang, C.Q.; Vermote, E.F.; Gao, F.; Channan, S.; Sexton, J.O.; Feng, M.; Narasimhan, R.; Kim, D.; et al. Global characterization and monitoring of forest cover using Landsat data: Opportunities and challenges. *Int. J. Digit. Earth* **2012**, *5*, 373–397. [CrossRef]

62. Popkin, G. How much can forest fight climate change? Trees are supposed to slow global warming, but growing evidence suggests they might not always be climate saviours. *Nature* **2019**, *565*, 280–282. [CrossRef]
63. Davin, E.L.; de Noblet-Ducoudré, N. Climatic Impact of global-scale deforestation: Radiative versus nonradiative processes. *J. Clim.* **2010**, *23*, 97–112. [CrossRef]
64. Kueppers, L.M.; Snyder, M.A.; Sloan, L.C.; Cayan, D.; Jin, J.; Kanamaru, H.; Kanamitsu, M.; Miller, N.L.; Tyree, M.; Du, H.; et al. Seasonal temperature responses to land-use change in the western United States. *Global Planet. Change* **2008**, *60*, 250–264. [CrossRef]
65. Liu, T.; Yu, L.; Bu, K.; Yan, F.; Zhang, S. Seasonal local temperature responses to paddy field expansion from rain-fed farmland in the cold and humid Sanjiang Plain of China. *Remote Sens.* **2018**, *10*, 2009. [CrossRef]
66. Liu, Z.; Notaro, M.; Gallimore, R. Indirect vegetation-soil moisture feedback with application to Holocene North Africa climate. *Global Change Biol.* **2010**, *16*, 1733–1743. [CrossRef]
67. Li, Y.; De Noblet-Ducoudré, N.; Davin, E.L.; Motesharrei, S.; Zeng, N.; Li, S.; Kalnay, E. The role of spatial scale and background climate in the latitudinal temperature response to deforestation. *Earth Syst. Dyn.* **2016**, *7*, 167–181. [CrossRef]
68. Li, D.; Wang, L. Sensitivity of surface temperature to land use and land cover change-induced biophysical changes: The scale issue. *Geophys. Res. Lett.* **2019**, *46*, 9678–9689. [CrossRef]